Book Chapter

A Theoretical Model of the Flow Properties of Postprocessed Direct Metal Laser Sintering Ti6Al4V (ELI)

AM Muiruri[1,2*], M Maringa[1*] and W du Preez[1*]

[1]Department of Mechanical and Mechatronics Engineering, Faculty of Engineering,Built Environment and Information Technology, Central University of Technology, South Africa
[2]Department of Mechanical Engineering, School of Engineering and Technology, South Eastern University Kenya, Kenya

***Corresponding Author:** AM Muiruri, Department of Mechanical and Mechatronics Engineering, Faculty of Engineering,Built Environment and Information Technology, Central University of Technology, Free State Private Bag X20539, Bloemfontein, South Africa

M Maringa, Department of Mechanical and Mechatronics Engineering, Faculty of Engineering,Built Environment and Information Technology, Central University of Technology, Free State Private Bag X20539, Bloemfontein, South Africa

W du Preez, Department of Mechanical and Mechatronics Engineering, Faculty of Engineering,Built Environment and Information Technology, Central University of Technology, Free State Private Bag X20539, Bloemfontein, South Africa

Published **April 18, 2023**

This Book Chapter is a republication of an article published by AM Muiruri, et al. at Advances in Materials Science and Engineering in November 2022. (AM Muiruri, M Maringa, W du Preez. A Theoretical Model of the Flow Properties of Postprocessed Direct Metal Laser Sintering Ti6Al4V (ELI). Advances in Materials Science and Engineering. Volume 2022, Article ID 4048913, 12 pages. https://doi.org/10.1155/2022/4048913)

How to cite this book chapter: AM Muiruri, M Maringa, W du Preez. A Theoretical Model of the Flow Properties of Postprocessed Direct Metal Laser Sintering Ti6Al4V (ELI). In: Esubalew Kasaw Gebeyehu, editor. Prime Archives in Material Science: 4th Edition. Hyderabad, India: Vide Leaf. 2023.

Abstract

Heat treatment of direct metal laser sintering (DMLS) Ti6Al4V (ELI) generates different mechanical properties of the alloy depending on the heat treatment cycle adopted. This is due to the different aspects of the microstructure, such as phase fraction, grain size, texture, and dislocation density, which vary with heat treatment. Other external factors, such as the prevailing level of strain, strain rate, and temperature, also affect the mechanical properties of the material. This paper presents the development of a theoretical model that couples the effects of strain rate, temperature, strain, grain size, and initial dislocation density to describe the flow properties of DMLS Ti6Al4V (ELI). According to the model, higher initial dislocation density results in higher yield stress, low strain hardening, and earlier saturation of flow stress. The model shows that the parabolic shape of the stress-strain curve of the alloy is dictated by the initial dislocation density, which is generally a factor of grain size.

1. Introduction

Additive manufacturing (AM) technology has allowed for the fast production of complex parts based on three-dimensional (3D) computer-aided design (CAD) model data without the need for complex tooling or machining. The technology is currently being adopted at different stages of product development, especially in the aircraft and biomedical industries, where it is deemed advantageous over conventional manufacturing processes [1–3]. It offers a high level of precision that traditional manufacturing techniques are incapable of matching and allows for flexible, intricate, and topology-optimised designs. It has also paved the way for the consolidation of existing part assemblies made from many pieces into a single part, thus streamlining the manufacturing process while improving the quality of its output [4, 5]. A typical example is the Leading-Edge Aviation Propulsion (LEAP) fuel nozzle of the jet engine, conventionally made from 20 different parts and now turned into a single part via AM, with a 25% reduction in weight [4]. Direct metal laser sintering (DMLS) and selective laser melting (SLM) are two of the various trademarks used for metal laser powder bed fusion (LPBF) technology that is currently being utilised for the production of commercial parts for use in the aircraft [5, 6] and biomedical industries [7], with prospects in automotive [8] and military sectors [9].

Despite the popularity and design benefits, metal AM is still limited by some major drawbacks such as the formation of nonequilibrium microstructure, residual stress, porosity, and poor surface quality. However, substantive efforts have been made to address these challenges. Heat treatment strategies to alleviate process-related macroresidual stresses, as well as the attainment of equilibrium microstructures for Ti6Al4V and therefore, improving the mechanical properties of the alloy, are available in the open literature [10–14]. Various methods of improving the surface quality of AM parts have been studied, some of which have been shown to reduce the surface roughness to as low as $R_a = 0.025\,\mu m$ [15]

from typical values of $R_a \approx 5\,\mu m$ and $R_z \approx 25\,\mu m$ [16], which qualifies as a superior mirror finish. The use of optimal AM process parameters has been shown to reduce and mitigate the formation of pores in the produced parts. For instance, the porosity of Ti6Al4V (ELI) parts produced by DMLS with optimised parameters has constantly been shown to be as low as 0.004% [11]. Where the porosity is too high, parts produced by the AM process can be subjected to post-processing to reduce the level of pores. The consecutive processes of heat treatment and hot isostatic pressing (HIP) were used to this end [12]. Kasperovich and Hausmann [12] reported a reduction of porosity from 0.077% to 0.012% after subsequent HIP treatment of AM specimens produced by optimised parameters.

The nonequilibrium microstructure of Ti6Al4V (ELI) formed during the DMLS process consists of fine α'-laths, commonly referred to as a martensitic grain within prior-β grains that are elongated along the build direction [11]. This kind of microstructure is characterised by a high yield strength of about 1100 MPa but limited ductility with a percentage elongation that is less than 10% [13]. The impact toughness of this microstructure has also been reported to be low, at a value of about 14 J. The required values of yield strength, percentage elongation, and impact toughness of Ti6Al4V for use in the aerospace industry are about 825 MPa, >10%, and 24 J, respectively [11]. Therefore, as-built DMLS Ti6Al4V (ELI) is undesirable for use where structural material toughness is critical, such as in the aerospace sector [17].

There is a need, therefore, to modify the metastable α' martensite microstructure of AM Ti6Al4V, which is achieved through postprocess heat treatment processes to satisfy the industrial requirements of mechanical performance. The heat treatment of Ti6Al4V alloy can be carried out in the region below or above the $\alpha \longrightarrow \beta$ transformation (transus) temperature, or as a combination of the two, depending on the desired microstructure. The $\alpha \longrightarrow \beta$-transus temperature for the Ti6Al4V alloy varies with the actual content of aluminium and vanadium [18] and is known to be 980°C for DMLS Ti6Al4V (ELI) [19].

The low-temperature heat treatment strategy in the subtransus region (usually at 650°C) is normally applied to alleviate macrothermal residual stresses in Ti6Al4V (ELI) resulting from the AM process and has little to no effect on the microstructure of the material [11, 13]. Complete decomposition of α' martensite of Ti6Al4V is only realised for annealing temperatures above 800°C [20, 21]. However, it is important to note that the complete decomposition of this microstructure is a function of heat treatment temperature and residence time [22]. A heat treatment temperature of 800°C for 4 hours has been reported in [20] to completely decompose α' DMLS martensite. During heat treatment, α' martensite transforms into a mixture of equilibrium α and β phases. The α laths in the mixture have an average width that varies depending on the heat treatment temperature and cooling rate [11–21] applied. The subtransus heat treatment does not lead to changes in the morphology of the prior-β grains. However super-transus heat treatment leads to decomposition and subsequent growth of columnar prior-β grains into equiaxed prior-β grains [15–21]. A combination of both subtransus and super-transus heat treatments and different cooling rates can be used to optimise the microstructure of the alloy. A more detailed analysis of the effects of different heat treatment strategies on the microstructure, dislocation densities, and crystallographic texture of DMLS Ti6Al4V (ELI) is covered in the authors' previous publications found in Reference [22, 23].

The load-bearing capacity of most engineering materials is usually assessed from their tensile properties, amongst other mechanical properties. The summary of the tensile properties of nonheat-treated and heat-treated DMLS Ti6Al4V (ELI) parts is shown in Table 1.

From the data presented in Table 1, it is evident that the mechanical properties of AM Ti6Al4V (ELI) depend on the specific heat treatment process adopted for the alloy. This is mainly because the heat treatment temperature affects the microstructural features of the alloy's phase fractions, grain morphology, the presence of defects, and the texture of prior -β grains [18–26]. While the texture of α-grains is mildly influenced by the heat treatment of AM parts [27], the phase fraction and the morphology of α-laths are greatly influenced by the annealing temperature and the rate of cooling, which in turn affect the mechanical properties of the alloy. Other than microstructural aspects, external factors, such as the prevailing level of strain rate and temperature, also influence the yield stress and deformation properties of metals and alloys.

Theoretical models can be used to predict the mechanical performance of the various forms of the DMLS Ti6Al4V (ELI) alloy and to design a material with specific mechanical properties, such as optimal strength and ductility, for use under a spectrum of external state variables. This can be achieved by understanding the yield and flow stress in terms of microstructural internal state variables and prevailing external state variables. A preliminary validation of the microstructural-based model with experimental data sets for different forms of heat-treated DMLS Ti6Al4V (ELI) was carried out and published in the authors' previous work, found in CUT Digital Respository [29]. In this paper, a complete theoretical constitutive model that is sensitive to the critical microstructural internal state variables and other external state variables is presented for predicting the yield stress and flow stress of various forms of DMLS Ti6A4V (ELI). The various model parameters are also analysed in this work.

2. A Microstructural Variable-Based Model for DMLS Ti6Al4V (ELI)

A suitable model to predict the stress-strain relationships of materials as a function of the prevailing levels of strain rate and temperature should provide a bridge between submicroscale phenomena and macroscale continuum mechanics. The flow diagram of the model proposed in this study is shown in Figure 1.

The envisaged model is classified into three parts: (i) prediction of yield stress (σ_y) as a function of grain size (d), strain rate ($\dot{\varepsilon}$), and temperature (T); (ii) subsequent

Table 1: Tensile properties of Ti6Al4V (ELI) parts built by DMLS and exposed to different heat treatment cycles [20, 24–28].

Condition	UTS (MPa)	YS (MPa)	El (%)	Ref
As-built	1211 ± 31	1100 ± 12	6.5 ± 0.6	[24]
	1265 ± 5	1098 ± 2	9.4 ± 0.5	[24]
Stress relieved	1170 ± 6	1098 ± 5	10.9 ± 0.8	[26]
	1052 ± 11	937 ± 9	9.6 ± 0.9	[25]
HT (730°C/2h/AC)	1046 ± 6	965 ± 16	9.5 ± 1	[25]
HT (950°C/1h/WQ)	1040 ± 4	925 ± 14	7.5 ± 14	[25]
HT (1050°C/1h/WQ)	951 ± 55	836 ± 64	7.9 ± 2	[25]
HT (800°C/2h/AC)	1073 ± 9	1010 ± 11	17.1 ± 1	[20]
HT (950°C/2h/AC)	984 ± 5	893 ± 3	14.2 ± 1.5	[20]
HT (1050°C/1h/AC)	988 ± 8	869 ± 4	13.3 ± 0.7	[21]
HT (1200°C/1h/AC)	988 ± 8	878 ± 7	11.3 ± 1.3	[20]
HT (1050°C/1h/WQ, followed by 990°C/0.5h/AC)	962 ± 12	838 ± 6	12 ± 0.1	[25]
HT (850°C/2h/FC)	1004 ± 6	955 ± 6	12.8 ± 1.4	[28]
HT (850°C/5h/FC)	965 ± 20	909 ± 24	Premature failure	[28]
HT (1015°C/0.5h/AC, followed by 843°C/2h/FC)	874 ± 23	801 ± 20	13.5 ± 1	[28]
HT (1020°C/2h/FC)	840 ± 27	760 ± 19	14.1 ± 3	[28]
HT (705°C/3h/FC)	1082 ± 34	1026 ± 35	9.1 ± 2	[28]
HT (940°C/1h/AC, followed by 650°C/2h/AC)	948 ± 27	899 ± 27	13.6 ± 0.3	[28]
HT (1015°C/0.5h/AC, followed by 730°C/2h/AC)	902 ± 19	822 ± 25	12.7 ± 0.6	[28]

WQ, water quenched; AC, air cooled; FC, furnace cooled; H, heat treated.

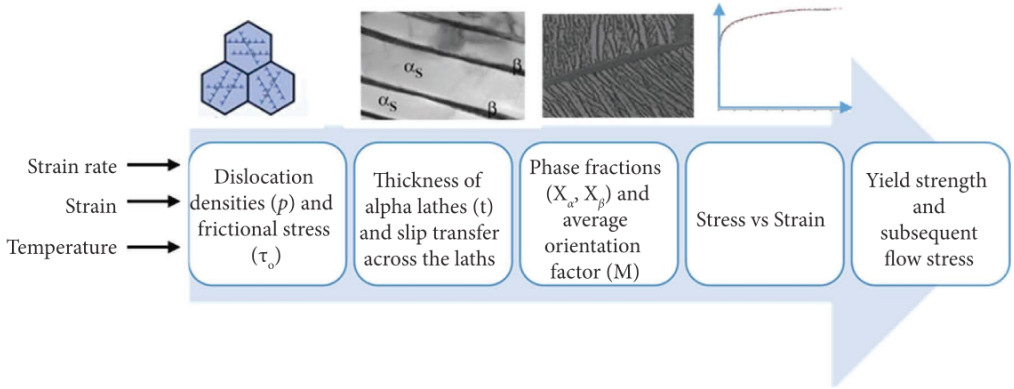

Figure 1: A flow diagram of the proposed microstructural variable-based model for predicting the mechanical properties of various forms of DMLS Ti6Al4V (ELI) alloy [29].

prediction of the flow stress (σ_p) as a function of equivalent plastic strain (ε_p), temperature (T), and dislocation density (ρ); and (iii) prediction of viscous drag (σ_{drag}) at high strain rate as a function of strain rate ($\dot{\varepsilon}$) and grain size (d). The total stress is, therefore, the sum of the three components of stress as follows:

$$\sigma = \sigma_y(d, \dot{\varepsilon}, T) + \sigma_p\left(\varepsilon_p, T, \rho\right) + \sigma_{\text{drag}}(\dot{\varepsilon}, d). \quad (1)$$

2.1. Prediction of Yield Stress. Grain boundary strengthening or Hall–Petch strengthening [30] can be used to determine the part of the yield stress (σ_d) that is dependent on the grain size, while the other part (σ_{mts}) can be determined from the mechanical threshold stress (MTS) formulation as a function of strain rate and temperature. Thus, the yield stress of a material can be expressed as follows:

$$\sigma_y = \sigma_d + \sigma_{\text{mts}} = \frac{K\_hp}{\sqrt{d}} + \sigma_{\text{mts}}, \quad (2)$$

where K_hp is the Hall–Petch constant and d denotes the average size of the grains. The parameter d is normally the shortest distance that mobile dislocations travel before encountering an obstacle (a grain boundary). It is important to note that depending on the heat treatment process applied to DMLS Ti6Al4V (ELI), the resultant microstructure can exist either as a lamellar, equiaxed, or bimodal microstructure. Thus, the parameter d in equation (2) is represented by the thickness of the α-laths in the case of lamellar microstructure or the diameter of the equiaxed α-grains in the case of equiaxed microstructure. Since the bimodal microstructure consists of both lamellar and equiaxed α-grains, the parameter d can be determined by the rule of mixture considering the relative fraction of each grain morphology; thus [31],

$$d = \left(\frac{V_{al}}{\sqrt{d_l}} + \frac{1 - V_{al}}{\sqrt{d_e}} \right), \tag{3}$$

where V_{al}, d_l, and d_e denote the volume fraction of the lamellar microstructure, the average thickness of the α-laths, and the average diameter of the equiaxed α-grains, respectively. It has been shown that the retained volume fraction of the β-phase in DMLS Ti6AL4V(ELI) samples heat treated to different temperatures of 800°C, 950°C and 1050°C, each with a residence time of 2 hours, is small and usually less than 10% [22, 23]. The retained β-phase shown in Figure 2 fills the small gaps between the α lamellae. Thus, the characteristic Hall–Petch strengthening mechanisms are more likely to occur in the α-phase, rather than the β-phase. It can also be speculated, as seen in Figure 2, that the α/β interface and the β layers themselves are analogous to the grain boundaries in single-phase materials.

Therefore, the grain boundary strengthening mechanism for materials where the volume fraction of β-phase is less than 10% [23] can be assumed to be controlled by the α-phase, and the contribution of the β-phase to the Hall–Petch and plastic deformation in general can be ignored [32]. However, if the volume fraction of β-phase is greater than 10%, the rule of the mixture as proposed in this study should apply, considering the effects of both phases on grain boundary strengthening as follows:

$$\sigma_d = K\_\mathrm{hp}\left(\left(\frac{V_\alpha}{\sqrt{d}} \right) + \left(\frac{1 - V_\alpha}{\sqrt{d_\beta}} \right) \right), \tag{4}$$

where V_α and d_β are the volume fraction of the α-phase and the average thickness of the β-grains, respectively.

The lattice stress (σ_i), which is the stress required to initiate slip, is sensitive to external state variables [33], where it increases with a rise in the applied strain rate and decreases with an increase in temperature. Therefore, the part of the yield stress that depends on temperature and strain rate can be expressed as proposed in [34] as follows:

$$\sigma_{\mathrm{mts}}(\dot{\varepsilon}, T) = (S\sigma_o)\frac{\mu(T)}{\mu_o}, \tag{5}$$

where S is the temperature and strain rate scaling factors of the yield stress, σ_o is the value of thermal stress at 0 K, μ is the shear modulus dependent on temperature, and μ_o is the shear modulus at absolute zero temperature (0 K). Using a combination of the existing relationship between free energy and the mechanical threshold stress (MTS) and the Arrhenius equation, the scaling factor S can be expressed as follow:

$$S = \left(1 - \left(\frac{k_b T}{g_{0i}\mu(T)b^3} \ln \frac{\dot{\varepsilon}_o}{\dot{\varepsilon}} \right)^{1\backslash q} \right)^{1\backslash p}, \tag{6}$$

where symbols k_b, b, T, $\dot{\varepsilon}$, and $\dot{\varepsilon}_o$ are the Boltzmann's constant, the Burgers vector, the test temperature, the test strain rate, and the reference strain rate, respectively. The term g_{0i} represents the normalised activation energy for dislocations to overcome the intrinsic barrier(s) [38]. Parameters p and q are model fitting constants. Combining equations (5) and (6) allows the total thermally activated stress to be expressed as follows:

$$\sigma_{\mathrm{mts}} = \sigma = \left(\frac{\mu(T)}{\mu_0} \right)\sigma^o \left(1 - \left(\left(\frac{k_b T}{g_{0i}\mu(T)b^3} \right) \ln \frac{\dot{\varepsilon}_o}{\dot{\varepsilon}} \right)^{1q} \right)^{1\backslash p}, \tag{7}$$

2.2. Strain Hardening and Prediction of Flow Stress. The Taylor strain hardening model can be used to predict the flow stress of a material as a function of increasing dislocation density during plastic deformation [39]. The Taylor strain hardening model for polycrystals is of the following form [40]:

$$\sigma - \sigma_y = \alpha\mu(T)bM\sqrt{\rho}, \tag{8}$$

where the symbols σ and σ_y denote the total stress and yield stress, respectively, and α is a dimensionless parameter of magnitude ranging from 0.2–0.4 for different materials. The symbol μ is the shear modulus, which is dependent on temperature (T), while b and ρ denote the Burgers vector and the average dislocation density, respectively. The symbol M is the Taylor factor, which relates the shear flow stress of a single crystal to the uniaxial flow stress of a polycrystal. The rate of accumulation of dislocation density with plastic strain can be expressed using a single differential equation with separate terms for generation and annihilation of dislocations, as proposed in [35] as follows:

$$\frac{\mathrm{d}\rho}{\mathrm{d}\varepsilon_p} = M(k_1\sqrt{\rho} - k_2\rho) = M(h - k_2\rho), \tag{9}$$

where k_1 and k_2 are coefficients for the accumulation and annihilation of dislocations, respectively, and h is a constant for athermal strain hardening. The increase in dislocation density in a material with plastic strain requires evaluation of the integral in equation (9), which yields the following expression:

$$\rho = M\left(\frac{h}{k_2}\left(1 - \exp\left(-k_2\varepsilon_p\right)\right) + \rho_o \exp\left(-k_2\varepsilon_p\right) \right), \tag{10}$$

where ρ_o is the average initial dislocation density in a material. Thus, the increase in flow stress with plastic strain from equations (8) and (10) is expressed as follows:

$$\sigma - \sigma_y = \alpha\mu(T)bM\left(\frac{h}{k_2}\left(1 - \exp\left(-k_2\varepsilon_p\right)\right) + \rho_o \exp\left(-k_2\varepsilon_p\right) \right)^{1/2}. \tag{11}$$

2.3. Prediction of the Viscous Drag Stress Component of Flow Stress. To increase the predictive capability of the model proposed in this study, a viscous drag component of stress is incorporated in the model to predict the deformation process of Ti6Al4V (ELI) at high strain rates. Various studies have found that the viscous drag effect at high strain rates slows the motion of dislocations in closed-packed structures, thus increasing the yield and flow stress of materials [41–43].

The viscous drag stress can be expressed as follows [42, 44]:

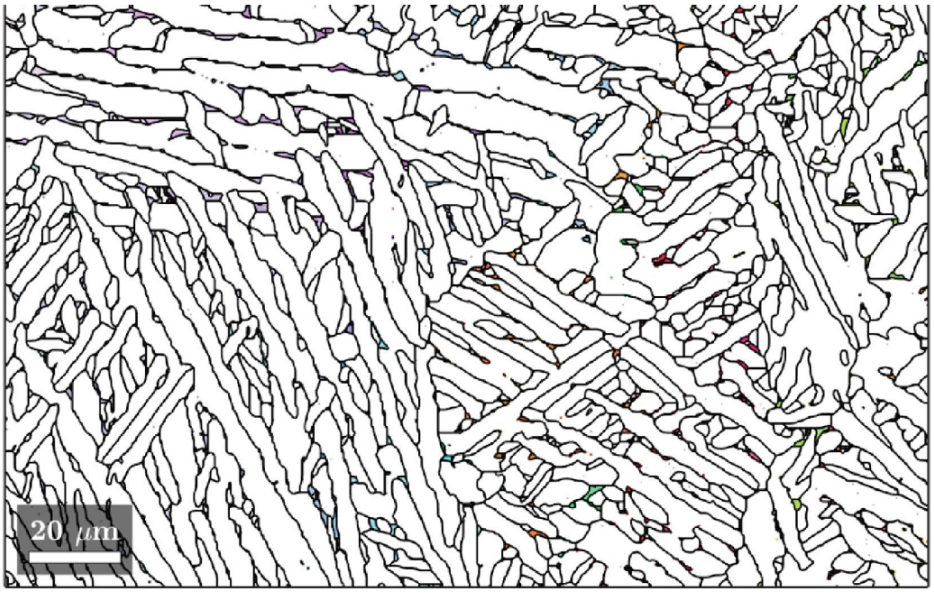

Figure 2: A microstructure of DMLS Ti6Al4V (ELI) was exposed to duplex annealing at 940°C for 2 h, then furnace cooled, followed by soaking at 750°C for 2 h, and then furnace cooled. The coloured small portions of the micrograph show the retained β-phase along the α-lath grain boundaries.

$$\sigma_{\text{drag}}\left(\dot{\varepsilon}_p\right) = \zeta.\left(1 - \exp\left(-\chi.\dot{\varepsilon}_p\right)\right), \tag{12a}$$

$$\chi = \left(\frac{M^2.\mu_d}{\rho_m.b^2.\sigma_a}\right), \tag{12b}$$

where the symbol χ represents the effective damping coefficient influencing the dislocation motion, while ζ is a material constant, both used as viscous drag curve fitting parameters. The symbols M, σ_a, μ_d, b, and ρ_m are the Taylor factor, athermal stress, drag coefficient, Burgers vector, and mobile dislocation density, respectively.

Grain sizes have a profound effect on the dislocation drag-controlled plasticity of materials [45]. The analysis of high strain rate flow stress curves of various forms of DMLS Ti6Al4V (ELI) in [46] demonstrated the relationship between flow stress and the grain size as one, where thicker grains give a higher drag stress and vice versa. The mobile dislocation density can be assumed to be proportional to the reciprocal of the average grain size (d) (taking this as the average lath thickness in the case of a lamellar microstructure and the diameter of the α-grains in the case of an equiaxed microstructure). Thus, the effective damping coefficient (χ) in equation (12b) can be modified as follows:

$$\chi = \left(\frac{M^2.\mu_d}{\rho_m.b^2.\sigma_a}\right) = \left(\frac{M^2.\mu_d.d}{b^2.\sigma_a}\right) = \omega.d, \tag{13a}$$

$$\omega = \frac{M^2.\mu_d}{b^2.\sigma_a}, \tag{13b}$$

where ω is the grain size dependent effective damping coefficient. Therefore, the viscous drag stress in equation (13a) can be expressed as a function of grain size as follows:

$$\sigma_{\text{drag}}\left(\dot{\varepsilon}_p, d\right) = \zeta.\left(1 - \exp\left(-\omega.d.\dot{\varepsilon}_p\right)\right). \tag{14}$$

3. Analysis of Various Model Parameters

3.1. Yield Stress Parameters. The grain size d determines the maximum distance mobile dislocations can travel before encountering an obstacle. The Hall–Petch relationship between the grain size-dependent yield stress (σ_d) and grain size (d) for the Ti6Al4V (ELI) alloy for a wide range of effective grain sizes, taking the Hall–Petch constant (K_hp) of the alloy as 0.328 MPa m$^{1/2}$ [32], is shown in Figure 3, where α-grains dominate deformation.

As seen in this figure, the yield stress for microstructures with different average grain sizes decreases as the average grain size increases. The first zone up to a grain size of about 2 μm is characterised by a sharp decrease in yield stress, beyond which the rate of decrease remains low and decreases gradually as the size of the grains increases.

3.2. Analysis of the Thermally Activated Component of Yield Stress. The use of equation (7), where different temperatures are accommodated, requires that the shear modulus be expressed as a function of temperature. The empirical relationship between shear modulus and temperature for Ti6Al4V is of the following form [36, 46]:

$$\mu(T) = 49.02 - \frac{5.821}{\exp^{(181/T)} - 1}\ (\text{GPa}). \tag{15}$$

A plot of equation 15 is shown in Figure 4(a), where the shear modulus is seen to decrease linearly as the temperature increases for the large part of the curve.

Some of the prescribed model parameters for the thermally activated stress in equation (6) for Ti6Al4V (ELI) were obtained from the literature as follows: $k_b = 1.38\,x\,10^{-23} J/K$, $b = 2.95\,x\,10^{-10} m$, $p = 1$, $q = 2$, and $\dot{\varepsilon}_o = 10^7\,s^{-1}$ [33, 36, 47]. The effects of the external state variables of temperature and strain rate and the normalised

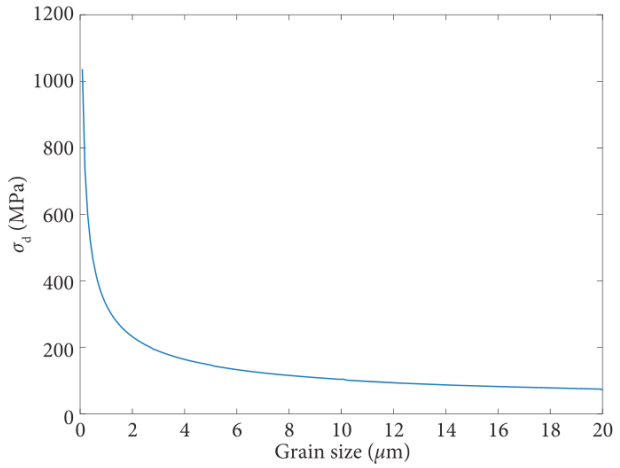

FIGURE 3: The Hall–Petch relationship for the Ti6Al4V (ELI) alloy for different effective average grain sizes.

thermal activation energy on the thermally activated stress are shown in Figures 4(b)–4(d). A range of temperatures of between 300 K and 700 K was used in Figure 4(b) as the maximum allowable temperature for Ti6Al4V alloy applications in industry is up to a value of about 695 K [48]. In Figure 4(b), the yield stress is shown to decrease almost linearly as the temperature increases, which is similar to the trend observed in Figure 4(a) for the variation of shear modulus with temperature. This decrease in yield stress and shear modulus as the temperature increases is due to the thermal activation of the motion of dislocations, resulting in an easier initiation of plastic flow or a reduction of Peierls stress at higher temperatures. Peierls stress is related to the temperature sensitivity of the yield stress of a material by the fact that increasing temperature weakens the atomic bond strength of a unit cell and therefore lowers the stress required to move a dislocation within the plane of atoms in a unit cell [49].

The increase in strain rate, on the other hand, is shown in Figure 4(c) and gives rise to an increase yield stress. This is mainly due to the instantaneous strain hardening expected at yield as the strain rate increases beyond that level. This increase is initially steep up to a strain rate of about 500 s^{-1}, after which the rate of increase decreases gradually, suggesting a decrease in the strain rate sensitivity of the material at higher strain rates. The strain rate sensitivity of materials is known to be higher at higher strain rates as the deformation changes from obstacle-controlled to obstacle and drag controlled at high strain rates [41–44]. The observations made in Figure 4(c) suggest that the MTS formulation is only adequate for strain rates below 500 s^{-1} and is on its own insufficient to accurately predict the upturn of flow stress at high strain rates, where the viscous drag phenomenon is expected to dominate deformation.

The yield stress in Figure 4(d) is also noted to increase as the parameter g_{0i} increases, which is expected because of the increase in the activation energy (a parameter that denotes the difficulty of deformation) of the active slip system in the material. It is important to note that although this parameter is a material property [38], it is known to be influenced by short-range obstacles, including alloying and interstitial elements in the case of Ti6Al4V [36]. This suggest that parameter g_{0i} will be the same for various microstructures of heat-treated DMLS Ti6Al4V (ELI) where the α-phase dominates plastic deformation.

3.3. Analysis of Strain Hardening. Dislocations are known to play a critical role in determining the plastic behaviour of materials and their flow stress under various loading conditions, such as strain rate and temperature. At high strain rates, Ti6Al4V (ELI) experiences instantaneous strain hardening, which increases the yield stress and subsequent flow stress of the material [45]. The movement and storage of dislocations during strain hardening are related to the external state variables shown in equation (11). Most of the parameters in this equation for the Ti6Al4V alloy can be obtained from the literature, while others depend on the microstructure.

The parameter α that depends on the geometrical arrangement of dislocations is approximately 0.2 for Ti6Al4V [27]. The shear modulus (μ) of the material is dependent on temperature and can be obtained from Figure 4(a). The Taylor factor (M) is dependent on the crystallographic texture of a material with reference to the loading axis. For randomly textured materials and based on the von Mises compatibility conditions (at least 5 independent slip systems are needed to accomplish deformation), Taylor [39] obtained a value for M of 3 for hcp crystal structures. Due to the relatively random texture of the α-phase for DMLS Ti6Al4V (ELI) alloy reported in [30], this value M was adopted for use in this study. However, it should be noted that approximate values of parameters M for different microstructures can be obtained if the Euler angles of all grains in a microstructure and the loading axis are known. The initial dislocation density (ρ_o) in a material is dependent on the microstructure and can be estimated by the method of X-ray diffraction or the use of transmission electron microscopy (TEM). The Burger's vector (b) for hcp Ti6Al4V can be taken as 0.295 nm [50]. The athermal work hardening coefficient (h) and the coefficient representing the rate of annihilation of dislocations (k_2) for the model are materially dependent and can be determined from experimental data.

The effects of these two last parameters, as well as those of temperature and initial dislocation density, on the shape of the flow curve in the plastic range were investigated here by varying one of the two parameters while holding all other parameters constant. The outcomes are discussed here. The curves in Figure 5 show the sensitivity of the flow stress with respect to the parameters h and k_2.

The two parameters are seen in this figure to have opposing effects on the predicted flow stress. Variation of the parameter h with a fixed dynamic recovery coefficient k_2 results in parabolic strain hardening, which together with the saturated flow stress decreases with decreasing value of the parameter h as seen in Figure 5(a). At a fixed value of the parameter h, larger values of the parameter k_2 result in smaller strain hardening and saturation flow stresses, as seen in Figure 5(b). These two parameters can be adjusted for a given material to fit experimental data.

The effect of temperature on the flow stress of Ti6Al4V (ELI) is investigated using equation (11) at temperatures ranging from −273°C to 800°C at fixed values of initial

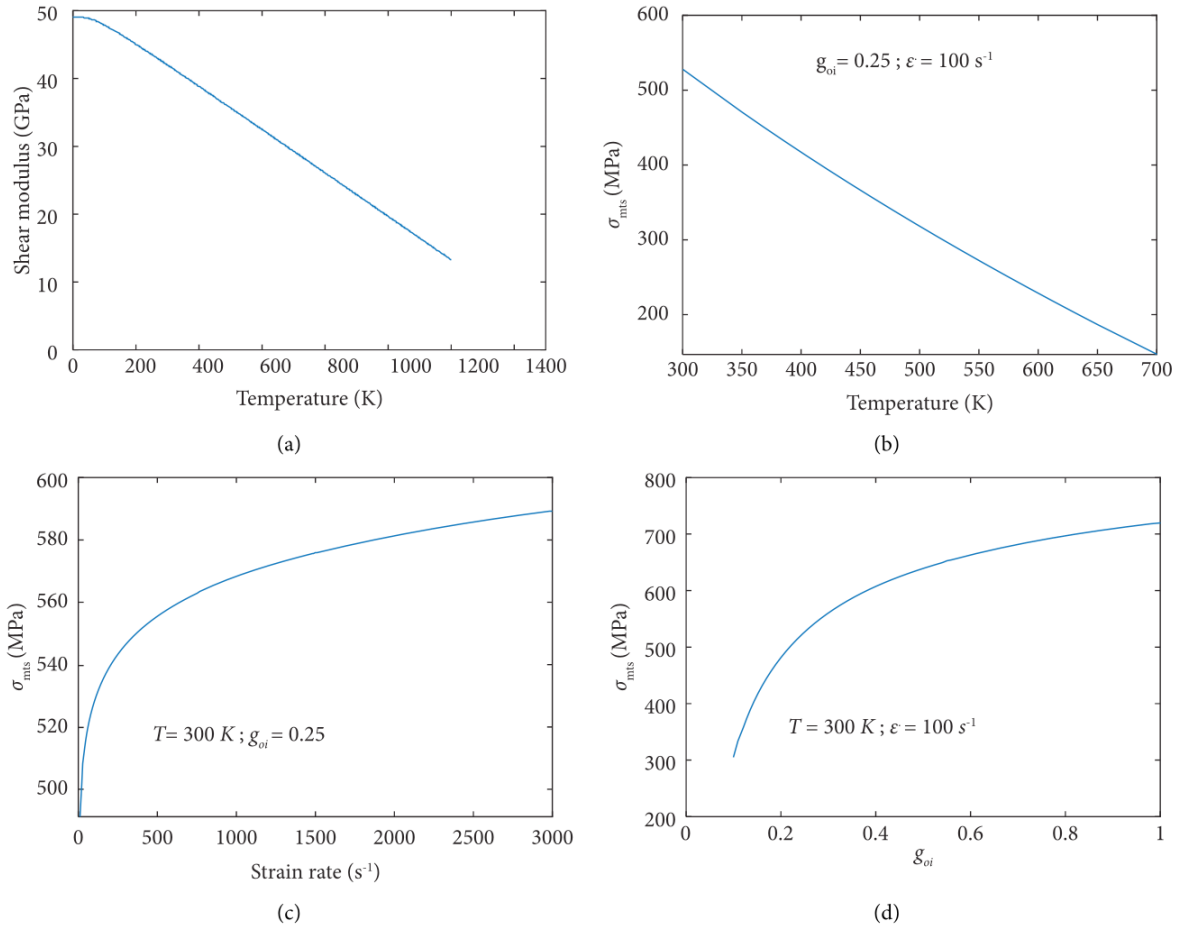

FIGURE 4: (a) The variation of shear modulus with temperature and (b), (c), and (d) the effects of temperature, strain rate, and normalised thermal activation energy on thermally activated stress.

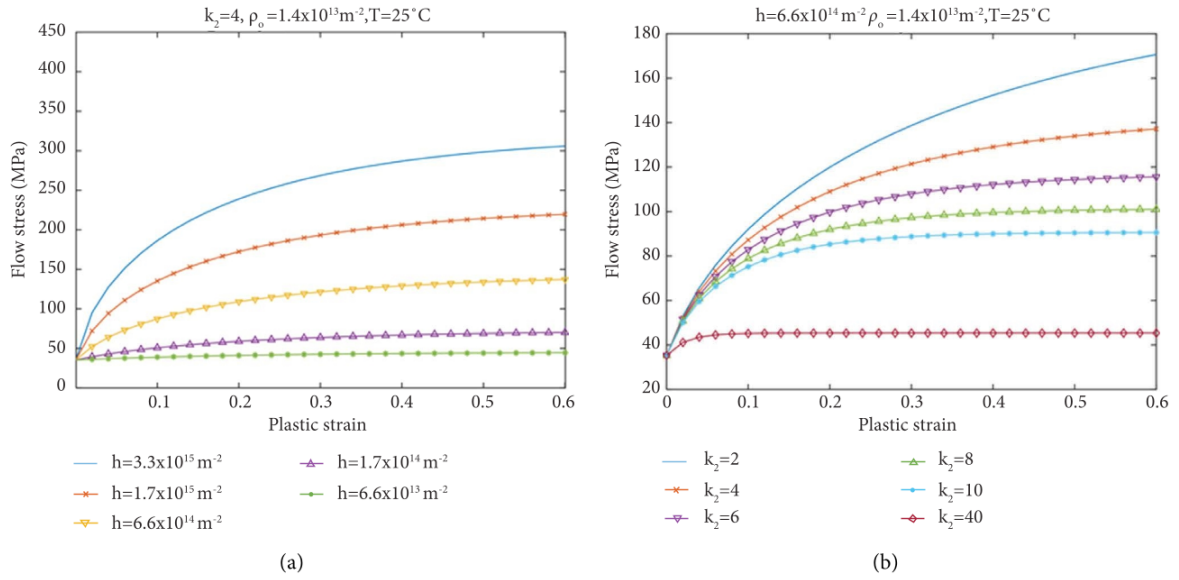

FIGURE 5: The effects of parameters (a) h and (b) k_2 on the shape of the flow stress curve.

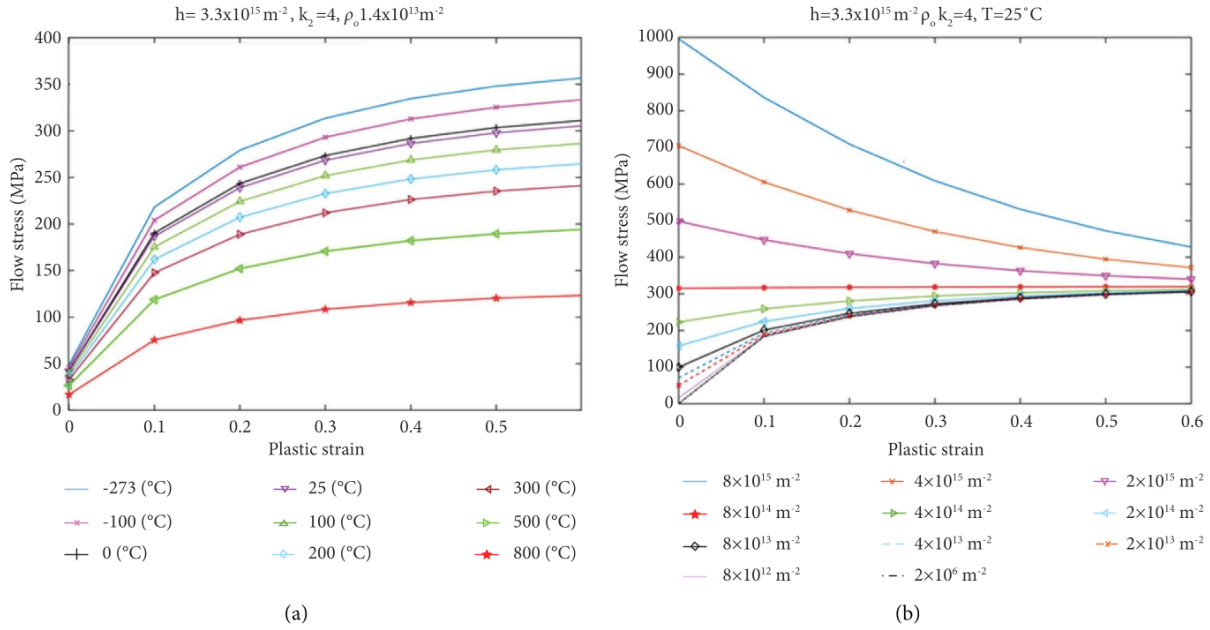

FIGURE 6: The effects of (a) temperature and (b) the initial dislocation density on the shape of the flow stress curve.

density (ρ_o) and parameters h and k_2, as seen in Figure 6(a). The curves in this figure show that an increase in temperature gives rise to a drop in flow stress. This is consistent with the physical reality, which dictates that the rate of recovery increases with increasing temperature.

It is important to note that the formulation of flow stress in equation (10) does not incorporate the failure criterion of the growth of damage in the alloy. Thus, the decrease in ductility that is expected to occur as the temperature decreases is not evident in Figure 6(a).

Figure 6(b) shows the effects of the initial dislocation density on the flow properties of the Ti6Al4V (ELI) alloy. The shape of the flow curves in this figure for very high initial dislocation densities in the material is a pronounced high start value that is followed by a drop in the flow stress or strain softening of the material with increasing plastic strain. The high start value of stress decreases with the decrease in the initial dislocation density, from a case where no strain hardening occurs to a case where strain hardening occurs. Clearly, the high density of dislocations in a material is known to increase its yield strength (peak stress). In fact, dislocations in materials will pile-up rapidly at barriers such as precipitates, grain boundaries, or even sessile dislocations. The leading dislocation in the pile-up is acted on not only by the applied shear stress but also by the interaction stress with other dislocations in the pile-up. High stresses initiate yielding on the other side of the barrier and can initiate cracks at the barriers [51], which could cause a decrease in the stress to cause strain softening at the onset of plastic flow as seen in Figure 6(b).

For dislocation densities below $8\,x\,10^{14}\,m^{-2}$, the flow curves are characterised by the familiar strain hardening that decreases in magnitude with increasing plastic strain. This is the common scenario for Ti6Al4V (ELI) alloys, as reported in [45], and is characteristic of metals and metal alloys. A further decrease in the initial dislocation density, according to the model, decreases the initial yield stress, and therefore the material has significant postyielding strain hardening before its rate decreases with the increase in strain. This is consistent with the physical reality where materials with large grain sizes have low yield stress, high ductility, and therefore low dislocation densities and have significant postyielding strain hardening [52].

3.4. Analysis of Viscous Drag Stress. The viscous drag stress can be assumed to be additive to the athermal component of the yield stress since the viscous drag effect resists the flow of dislocations and thus increases the yield stress and subsequently the flow stress. Generally, dislocation drag springs from electrons and phonons in materials and has a retarding effect on the movement of dislocations as a Newtonian drag force [41–44]. Because of the viscous drag, the kinetic energy of dislocations is reduced, which otherwise would help overcome obstacles, and more external force is thus required to keep the dislocations in motion. With the addition of viscous drag stress, the physical mechanism behind the upturn of yield and flow stress at high strain rates can be accommodated.

From equation (14), the viscous drag stress is seen to be a function of strain rate (an external state variable) and grain size (an internal state variable). Parameters ζ and ω in equation (14) are material constants that can be determined from experimental data. The effects of these four parameters on viscous drag stress are presented in Figure 7.

It is evident from the curves in this figure that as the strain rate increases, the viscous drag stress becomes relevant and quickly rises with the deformation rate for all values of calibration parameters ζ and ω, and grain size (d). However, it is important to note that at low and moderate strain rates ($\dot{\varepsilon} < 100\,s^{-1}$), the viscous drag component is

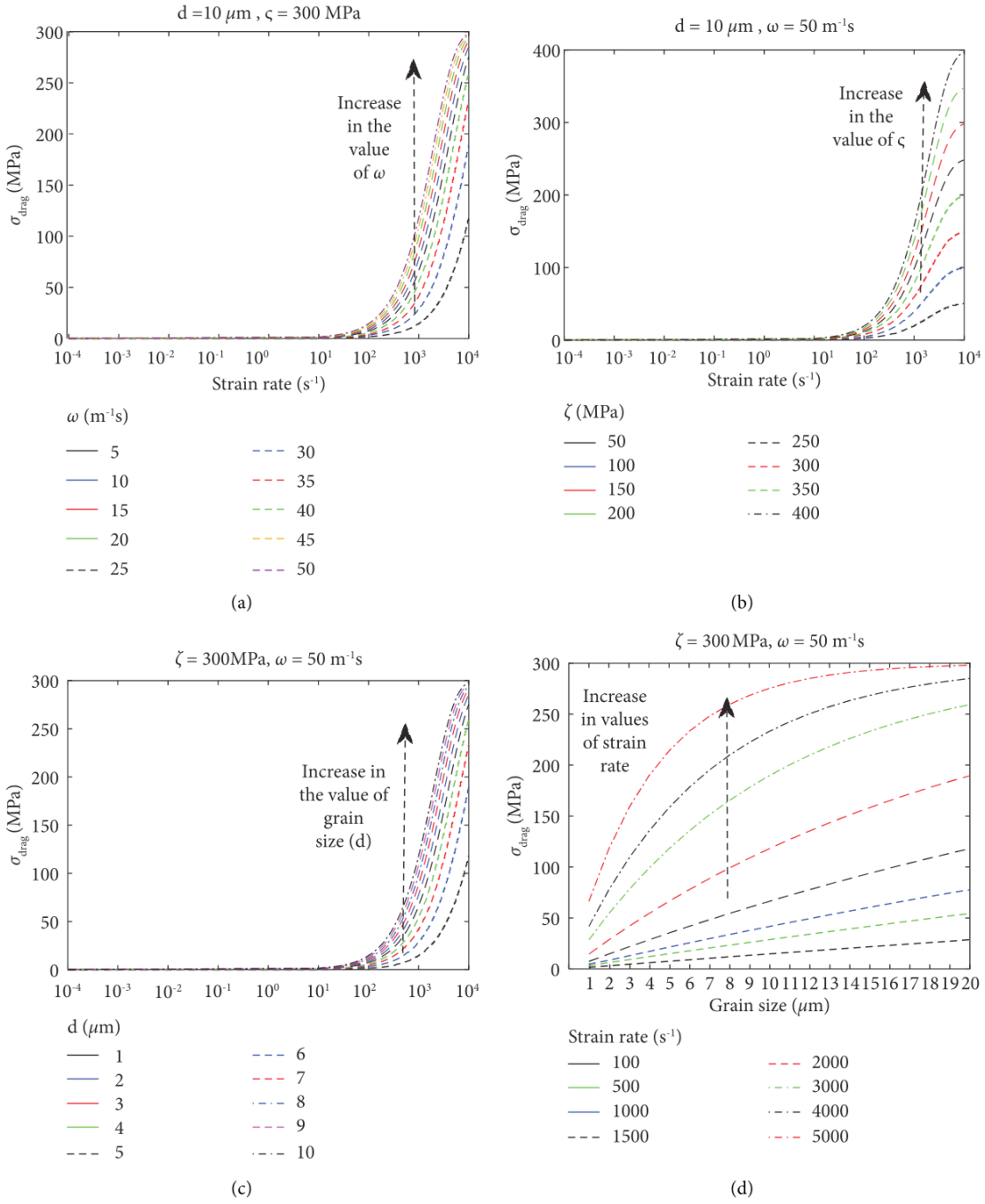

FIGURE 7: The effects of various model parameters (a) ω, (b) ζ, (c) grain size, and (d) strain rate on viscous drag stress.

small and negligible at all values of ζ, ω, and d. The low values of viscous drag at first led to the conclusion that the deformation was mainly controlled by obstacles. The increase in the values of the curve fitting parameters ω and ζ, grain size, and strain rate all lead to an increase in viscous drag stress, as shown in Figures 7(a)–7(d), respectively, although the effect of strain rate is clearly seen in this figure to be predominant.

4. Conclusions

By examining various mechanisms that play a critical role in the yield point and plastic flow in the Ti6Al4V alloy, a theoretical constitutive relationship was successfully adopted to provide a macroscopic description of the flow properties of various forms of LPBF Ti6Al4V (ELI) over a wide range of external state variables. The following conclusions arise from this study:

(i) The average grain size and initial dislocation density are the critical microstructural aspects that influence the yielding and deformation properties of a material. Therefore, they are important internal state variable input parameters in the formulation of the theoretical model for flow stress.

(ii) The utility of the MTS formulation that relates yield stress to strain rate and temperature is only limited to low and moderate strain rates and cannot be used alone to accurately predict yield stress at high strain rates.

(iii) The shape of the strain hardening curve is influenced by the athermal strain hardening coefficient h , dislocation annihilation coefficient, initial dislocation density of a material, and temperature.

(iv) Parameter h results in parabolic shapes for flow stress curves, and its increase leads to an increase in the value of saturation flow stress. Parameter k_2 has an opposite effect to that of parameter h where an increase in its value results in lower strain hardening and saturation flow stresses.

(v) The initial dislocation density in a material determines the initial high stresses and the extent of strain softening or strain hardening postyielding, affecting the parabolic shape of the flow stress curve.

(vi) The viscous drag stress is greatly influenced by the level of strain rate and grain size and increases in magnitude with increasing values of each of these two parameters.

(vii) The viscous drag stress is insignificant at low to moderate strain rates ($\dot{\varepsilon} < 100\, s^{-1}$).

Future studies should aim at testing and validating the complete proposed model with experimental data. A numerical analysis should also be conducted to test the utility of the model for a wide range of internal and external state variables. While the proposed model presented in this study only considered the DMLS Ti6Al4V (ELI) alloy, future research should also aim at extending the utility of the model to more materials that are used in structural applications, such as steel and aluminium-based alloys.

Data Availability

The datasets presented in this study are available on request from the corresponding author and are not publicly available as they form part of ongoing research.

Disclosure

The research presented in this paper forms part of the corresponding author's Doctoral thesis, which is available in the Central University of Technology digital repository [47]. The title and abstract of this paper were submitted to the 6th World Congress on Integrated Computational Materials Engineering (ICME 2022): On-Demand Oral Presentation.

Conflicts of Interest

The authors declare that there are no conflicts of interest.

Acknowledgments

This research was funded by the South African Department of Science and Innovation (DSI) through the Council for Scientific and Industrial Research (CSIR) for the Collaborative Program in Additive Manufacturing (CPAM).

References

[1] S. Sarat, L. Yifan, H. Andrew, R. Chalk, W. Thomas, and D. Jordison, "Additive manufacturing for the aircraft industry: a review," *Journal of Aeronautics & Aerospace Engineering*, vol. 8, no. 215, 2019.

[2] A. Arjunan, M. Demetriou, A. Baroutaji, and C. Wang, "Mechanical performance of highly permeable laser melted Ti6Al4V bone scaffolds," *Mechanical Behavior of Biomedical Materials*, vol. 102, Article ID 103517, 2020.

[3] K. Bari and A. Arjunan, "Extra low interstitial titanium based fully porous morphological bone scaffolds manufactured using selective lased melting," *Journal of the Mechanical Behavior of Biomedical Materials*, vol. 96, pp. 1–12, 2019.

[4] S. Yang, Y. Tang, and Y. F. Zhao, "A new part consolidation method to embrace the design freedom of additive manufacturing," *Journal of Manufacturing Processes*, vol. 20, no. 3, pp. 444–449, 2015.

[5] S. Kim and S. K. Moon, "A part consolidation design method for additive manufacturing based on product disassembly complexity," *Applied Sciences*, vol. 10, no. 3, p. 1100, 2020.

[6] A. Katz-Demyanetz, V. V. Popov, A. Kovalevsky, D. Safranchik, and A. Koptyug, "Powder-bed additive manufacturing for aerospace application: techniques, metallic and metal/ceramic composite materials and trends," *Manufacturing Review*, vol. 6, no. 5, p. 5, 2019.

[7] F. Calignano, M. Galati, L. Iuliano, and P. Minetola, "Design of additively manufactured structures for biomedical applications: a review of the additive manufacturing processes applied to the biomedical sector," *Journal of Healthcare Engineering*, vol. 2019, Article ID 9748212, 2019.

[8] S. Hendrixson, "Real Examples of 3D Printing in the Automotive Industry," 2021, https://www.mmsonline.com/articles/real-examples-of-3d-printing-in-the-automotive-industry.

[9] C. Megan, "Military Starts to Run with 3D Printing and Additive Manufacturing," 2021, https://www.militaryaerospace.com/home/article/14205856/military-starts-to-run-with-3d-printing-and-additive-manufacturing.

[10] Z. Y. Zhao, L. Li, P. K. Bai et al., "The heat treatment influence on the microstructure and hardness of TC4 titanium alloy

manufactured via selective laser melting," *Materials*, vol. 11, no. 8, p. 1318, 2018.

[11] A. Muiruri, M. Maringa, W. du Preez, and L. Masu, "Effects of stress-relieving heat treatment on impact toughness of direct metal laser sintering (DMLS)-Produced Ti6Al4V (ELI) parts," *Journal of Occupational Medicine*, vol. 72, no. 3, pp. 1175–1185, 2020.

[12] G. Kasperovich and J. Hausmann, "Improvement of fatigue resistance and ductility of TiAl6V4 processed by selective laser melting," *Journal of Materials Processing Technology*, vol. 220, pp. 202–214, 2015.

[13] A. Muiruri, M. Maringa, W. du Preez, and L. Masu, "Effect of stress-relieving heat treatment on the high strain rate dynamic compressive properties of additively manufactured Ti6Al4V (ELI)," *Metals*, vol. 10, p. 653, 2020.

[14] C. V. Funch, A. Palmas, K. Somlo et al., "Targeted heat treatment of additively manufactured Ti6Al4V for controlled formation of bi-lamellar microstructures," *Journal of Materials Science & Technology*, vol. 81, pp. 67–76, 2021.

[15] N. N. Kumbhar and A. V. Mulay, "Post processing methods used to improve surface finish of products which are manufactured by additive manufacturing technologies: a review," *Journal of the Institution of Engineers: Series C*, vol. 99, pp. 481–487, 2018.

[16] G. M. Moletsane, "Microstructure and Mechanical Properties of Ti6Al4V(ELI) Parts Produced by DMLS," Master's Dissertation, Central University of Technology, Bloemfontein, South Africa, 2016.

[17] L. F. Monaheng, W. B. du Preez, and C. Polese, "Towards qualification in the aviation industry: impact toughness of Ti6Al4V(ELI) specimens produced through laser powder bed fusion followed by two-stage heat treatment," *Metals*, vol. 11, no. 11, p. 1736, 2021.

[18] T. Ahmed and H. J. Rack, "Phase transformations during cooling in α+β titanium alloys," *Materials Science and Engineering A*, vol. 243, no. 1-2, pp. 206–211, 1998.

[19] Y. Yang, Y. Liu, J. Chen et al., "Crystallographic features of α variants and β phase for Ti6Al4V alloy fabricated by selective laser melting," *Materials Science and Engineering A*, vol. 707, pp. 548–558, 2017.

[20] Q. Huang, X. Liu, X. Yang, R. Zhang, Z. Shen, and Q. Feng, "Specific heat treatment of selective laser melted Ti6Al4V for biomedical applications," *Frontiers of Materials Science*, vol. 9, no. 4, pp. 373–381, 2015.

[21] D. D. Markovitz, A. Katsman, A. Shirizly, and M. Bamberger, "Microstructure and mechanical properties of heat-treated selective laser melting manufactured Ti6Al4V," in *Proceedings of the ICANM: International Conference & Exhibition on Advanced & Nano Materials*, pp. 33–42, Ottawa, Canada, August 2015.

[22] A. Muiruri, M. Maringa, and W. du Preez, "Crystallographic texture analysis of as-built and heat-treated Ti6Al4V (ELI) produced by direct metal laser sintering," *Crystals*, vol. 10, p. 699, 2020.

[23] A. Muiruri, M. Maringa, and W. du Preez, "Evaluation of dislocation densities in various microstructures of additively manufactured Ti6Al4V (eli) by the method of X-ray diffraction," *Materials*, vol. 13, p. 5355, 2020.

[24] F. Gil Mur, D. Rodriguez, and J. Planell, "Influence of tempering temperature and time on the α'-Ti-6Al-4V martensite," *Journal of Alloys and Compounds*, vol. 234, no. 2, pp. 287–289, 1996.

[25] T. Vilaro, C. Colin, and J. D. Bartout, "As-fabricated and heat-treated microstructures of the Ti-6Al-4V alloy processed by selective laser melting," *Metallurgical and Materials Transactions A*, vol. 42, no. 10, pp. 3190–3199, 2011.

[26] M. G. Moletsane, P. Krakhmalev, N. Kazantseva, A. du Plessis, I. Yadroitsava, and I. Yadroitsev, "Tensile properties and microstructure of direct metal laser-sintered Ti6Al4V(ELI) alloy," *South African Journal of Industrial Engineering*, vol. 27, no. 3, pp. 110–121, 2016.

[27] M. Simonelli, Y. Y. Tse, and C. Tuck, "The formation of $\alpha + \beta$ microstructure in as-fabricated selective laser melting of Ti6Al4V," *Journal of Materials Research*, vol. 29, no. 17, pp. 2028–2035, 2014.

[28] B. Vrancken, L. Thijs, J. P. Kruth, and J. Van Humbeeck, "Heat treatment of Ti6Al4V produced by selective laser melting: microstructure and mechanical properties," *Journal of Alloys and Compounds*, vol. 541, pp. 177–185, 2012.

[29] CUT Digital Repository, "CUT Digital Repository," 2017, https://urldefense.com/v3/__http://ir.cut.ac.za/bitstream/handle/11462/2368/Muiruri%2c%20Amos%20Mwangi.pdf?isAllowed=y&sequence=1__;JSUl!!N11eV2iwtfs!paKcogTp3vFOOX8mLsWdWPzjdP0z_CT8cNzrqlTxK09fDnc2NHAI2mXZwE2itrImqu9zn3xjgveeZol3bEihK1Mcg-vlyXgNsQ%24.

[30] E. O. Hall, "The deformation and ageing of mild steel: III discussion of results," *Proceedings of the Physical Society Section B*, vol. 64, no. 9, pp. 747–753, 1951.

[31] M. Galindo-Fernández, K. Mumtaz, P. Rivera-Diaz-del-Castillo, E. Galindo-Nava, and H. Ghadbeigi, "A microstructure sensitive model for deformation of Ti6Al4V describing cast-and-wrought and additive manufacturing morphologies," *Materials & Design*, vol. 160, pp. 350–362, 2018.

[32] D. H. Kohn and P. Ducheyne, "Tensile and fatigue strength of hydrogen-treated Ti6Al4V alloy," *Journal of Materials Science*, vol. 26, no. 2, pp. 328–334, 1991.

[33] S. Nemat-Nasser, W. G. Guo, V. F. Nesterenko, S. Indrakanti, and Y. B. Gu, "Dynamic response of conventional and hot isostatically pressed Ti–6Al–4V alloys: experiments and modeling," *Mechanics of Materials*, vol. 33, no. 8, pp. 425–439, 2001.

[34] U. Kocks, "Realistic constitutive relations for metal plasticity," *Materials Science and Engineering A*, vol. 317, no. 1–2, pp. 181–187, 2001.

[35] H. Mecking and U. Kocks, "Kinetics of flow and strain-hardening," *Acta Metallurgica*, vol. 29, no. 11, pp. 1865–1875, 1981.

[36] R. Picu and A. Majorell, "Mechanical behavior of Ti–6Al–4V at high and moderate temperatures—Part II: constitutive modeling," *Materials Science and Engineering A*, vol. 326, no. 2, pp. 306–316, 2002.

[37] A. Rusinek, J. A. Rodrıguez-Martınez, and A Arias, "A thermo-viscoplastic constitutive model for FCC metals with application to OFHC copper," *International Journal of Mechanical Sciences*, vol. 52, no. 2, pp. 120–135, 2010.

[38] U. F. Kocks, "Laws for work-hardening and low-temperature creep," *Journal Of Engineering Materials And Technology*, vol. 98, no. 1, pp. 76–85, 1976.

[39] G. I. Taylor, "The mechanism of plastic deformation of crystals. Part 1–Theoretical," *Proceeding of the Material Society A, Mathematical, Physical and Engineering Sciences*, vol. 145, no. 855, 1934.

[40] M. Kassner, "Taylor hardening in five-power-law creep of metals and class M alloys," *Acta Materialia*, vol. 52, no. 1, pp. 1–9, 2004.

[41] R. Kapoor and S. Nemat-Nasser, "Comparison between high and low strain-rate deformation of tantalum," *Metallurgical*

and Materials Transactions A, vol. 31, no. 13, pp. 815–823, 2000.

[42] H. J. Frost and M. F. Ashby, *Deformation-mechanism Maps: The Plasticity and Creep of Metals and Ceramics*, pp. 134–147, Elsevier Science Ltd, Michigan, MI, USA, 1982.

[43] T. Vreeland and K. Jassby, "Temperature dependent viscous drag in close-packed metals," *Materials Science and Engineering*, vol. 7, no. 2, pp. 95–102, 1971.

[44] D. R Lesuer, G. Kay, and M. M. LeBlanc, *Modelling Large-Strain, High-Rate Deformation in Metals*, Third Biennial Trilaboratory Engineering Conference on Modelling and Simulation, Pleasanton, CA, USA, 2001.

[45] Z. Mao, X. N. An, X. Liao, and J. Wang, "Opposite grain size dependence of strain rate sensitivity of copper at low *vs*. high strain rates," *Materials Science and Engineering A*, vol. 738, pp. 430–438, 2018.

[46] A. Muiruri, M. Maringa, and W. du Preez, "High strain rate properties of various forms of Ti6Al4V(ELI) produced by direct metal laser sintering," *Applied Sciences*, vol. 11, no. 17, p. 8005, 2021.

[47] C. H. Park, Y. I. Son, and C. S. Lee, "Constitutive analysis of compressive deformation behavior of ELI-grade Ti–6Al–4V with different microstructures," *Journal of Materials Science*, vol. 47, no. 7, pp. 3115–3124, 2012.

[48] AzoM, "Properties: Titanium alloys—Ti6Al4V grade 5—AzoM.com," 2020, https://www.azom.com/properties.aspx?ArticleID=1547.

[49] R. Peierls, "The size of a dislocation," *Proceedings of the Physical Society*, vol. 52, no. 1, pp. 34–37, 1940.

[50] D. Hull and D. J. Bacon, *Introduction to Dislocations*, pp. 205–217, Elsevier, Amsterdam, The Netherlands, 2011.

[51] J. Shi and M. Zikry, "Grain-boundary interactions and orientation effects on crack behavior in polycrystalline aggregates," *International Journal of Solids and Structures*, vol. 46, no. 21, pp. 3914–3925, 2009.

[52] D. M. Xu, X. L. Wan, J. X. Yu, G. Xu, and G. Q. Li, "Effect of grain refinement on strain hardening and fracture in austenitic stainless steel," *Materials Science and Technology*, vol. 34, no. 11, pp. 1344–1352, 2018.